

Anomalous Transition Magnetic Moments in two-dimensional Dirac Materials

Sanghita Sengupta,¹ Madalina I. Furis,^{2,3} Oleg P. Sushkov,⁴ and Valeri N. Kotov^{3,2}

¹*Institut Quantique and Département de Physique,*

Université de Sherbrooke, Sherbrooke, Québec, Canada J1K 2R1

²*Materials Science Program, University of Vermont, Burlington, VT 05405*

³*Department of Physics, University of Vermont, Burlington, VT 05405*

⁴*School of Physics, University of New South Wales, Sydney 2052, Australia*

(Dated: December 15, 2021)

We show that the magnetic response of atomically thin materials with Dirac spectrum and spin-orbit interactions can exhibit strong dependence on electron-electron interactions. While graphene itself has a very small spin-orbit coupling, various two-dimensional (2D) compounds “beyond graphene” are good candidates to exhibit the strong interplay between spin-orbit and Coulomb interactions. Materials in this class include dichalcogenides (such as MoS₂ and WSe₂), silicene, germanene, as well as 2D topological insulators described by the Kane-Mele model. We present a unified theory for their in-plane magnetic field response leading to “anomalous”, i.e. electron interaction dependent transition moments. Our predictions can be potentially used to construct unique magnetic probes with high sensitivity to electron correlations.

I. INTRODUCTION

Two-dimensional quantum materials are characterized by low-energy quasiparticle excitations that can be fully described by an effective (2+1)-dimensional Dirac equation. Naturally, various quantum electrodynamics (QED) phenomena associated with Dirac physics manifest themselves in these quantum condensed matter systems¹⁻⁴ even though the Dirac quasiparticles have non-relativistic nature and arise purely from band structure considerations.

One such astonishing feature associated with this class of materials is their magnetic response. In the presence of a magnetic field, the Dirac fermions exhibit a plethora of quantum phases which can range from anomalous quantum Hall states^{5,6} to quantum holography in graphene flakes⁷. While most studies related to anomalous quantum Hall physics have been conducted within the context of massless 2D Dirac fermions^{5,6,8,9}, recent research elucidates similar magnetic phenomena arising in the regime of massive 2D Dirac fermions^{10,11}.

In this paper we explore the magnetic response of the massive 2D Dirac fermions, with a special focus on the effect of electron-electron interactions. The candidate materials for this study include: (i) quantum Spin Hall (QSH) insulator states described by the Kane-Mele model¹², (ii) atomically thin semiconductor family of transition metal dichalcogenides (TMDCs)^{13,14} and (iii) topological insulator family of Silicene-Germanene class of materials^{15,16}.

Our chosen materials are characterized by gapped Dirac spectrum. In the case of QSH states described by the Kane Mele model, it was shown that the symmetry allowed spin-orbit coupling (SOC) leads to an opening of the energy gap in the linear, gapless electronic dispersion of graphene¹². This SOC thus converts the 2D semi-metallic graphene into a 2D topological insulator with gapless edge modes, while being insulating in the bulk. These QSH states thus allow for the generation of

dissipationless spin currents and are a topic of immense interest^{12,17,18}. However, it was also pointed out that while the SOC in graphene is of the order of 4 meV, the gap generated by it is rather small, of the order of $\sim 10^{-3}$ meV^{19,20}. One of the goals of the present work is to study in detail the in-plane magnetic response of the Kane Mele model where we show that Coulomb interactions can have quite significant effect and lead to enhanced spin flip (transition) magnetic moment.

Our theoretical approach is conceptually similar to calculations performed in relativistic QED^{21,22} where Schwinger’s celebrated vertex correction to the Dirac electron magnetic form factor translates into anomalous (fine structure constant dependent) g-factor. Of course all materials considered in this work are non-relativistic systems with effective Dirac quasiparticles; thus any “anomalous” corrections to spin response will originate from the Coulomb interaction between quasiparticles. Naturally, the results for the Kane Mele model and the other 2D systems with SOC will be anisotropic since it is well known that all of them exhibit strong intrinsic spin anisotropy, with the spin z-component (perpendicular to the planes) conserved. This means that only *in-plane* magnetic fields, leading to off-diagonal (spin flip) transitions, can give rise to anomalous, i.e. Coulomb interaction dependent *transition* magnetic moments. We also point out that interaction-dependent magnetic moments have recently been studied for three dimensional Dirac and Weyl insulators²³. Compared to those systems, the spin response of 2D materials with SOC is also, naturally, quite different and we describe it in detail in this work.

As mentioned before, we will also extend and apply our formalism and calculations of anomalous transition magnetic moments to two other systems which include the atomically thin TMDCs and Silicene-Germanene class of materials. Besides being gapped, these materials also display strong intrinsic spin-orbit coupling effects^{14,24-33}. Thus the interplay of electron-electron interactions and SOC in these systems is a topic of great interest.

The general structure of the paper is as follows: we will begin with the Kane Mele model in Sec. II, providing the general methodology and results for the one-loop correction to the transition magnetic moment. We will then adapt and extend this formalism to TMDCs and Silicene-Germanene class of materials in Sec. III and Sec. IV. Finally we will conclude in Sec. V with an outlook that summarizes our results. We also discuss possible experimental probes for detection of the interaction effects calculated in this work.

II. EFFECT OF COULOMB INTERACTIONS ON TRANSITION (SPIN-FLIP) MAGNETIC MOMENT WITHIN THE KANE MELE MODEL

The Kane Mele model describes the general 2D Dirac Hamiltonian with a mass term that originates from the spin-orbit coupling. This SOC renders the system as gapped and much of this section will be devoted to understanding the effect of Coulomb interaction on the SOC. Let us begin with the general procedure to calculate the one-loop correction to transition moment for this model. The Hamiltonian of the Kane Mele model¹² is,

$$H = v\sigma \cdot \mathbf{k} + \lambda\sigma_z s_z. \quad (1)$$

where v is the Fermi velocity in the material, the real spin of the fermion is $s_z = \pm 1$, for spin up and spin down. $\hat{\sigma}_i$ represents the pseudospin associated with the Pauli spin matrices in the valleys and the spin-orbit coupling is given by λ . In our derivations we choose the convenient natural units $\hbar = v = 1$, unless otherwise mentioned. From the Hamiltonian we can see that the spin in the z channel is always conserved. This means that interaction corrections to the diagonal (same spin) transitions are forbidden, while spin-flip transitions (caused by magnetic field in the S_x (or S_y) direction) can acquire anomalous components. Without loss of generality, in this and the next sections, we work in a given valley (already assumed in the above Hamiltonian). It is easy to see that the results for the spin response are valley independent (which also applies to the interaction corrections since the long-range Coulomb interaction does not mix valleys.) We will also be assuming, in this and all other sections, that the system always remains an insulator (i.e. the chemical potential is in the gap).

Within the hamiltonian of the Kane Mele model, the dispersion relation ε_k and eigenfunctions at momentum k are given as

$$\varepsilon_k = \sqrt{k^2 + \lambda^2}, \quad (2)$$

$$|\uparrow\rangle = \Psi(k)^{+1} = \frac{k}{\sqrt{2}\sqrt{\varepsilon^2 - \lambda^2}} \begin{pmatrix} 1 \\ \frac{\varepsilon - \lambda}{(k_x - ik_y)} \end{pmatrix}, \quad (3)$$

$$|\downarrow\rangle = \Psi(k)^{-1} = \frac{k}{\sqrt{2}\sqrt{\varepsilon^2 + \lambda^2}} \begin{pmatrix} 1 \\ \frac{\varepsilon + \lambda}{(k_x - ik_y)} \end{pmatrix}. \quad (4)$$

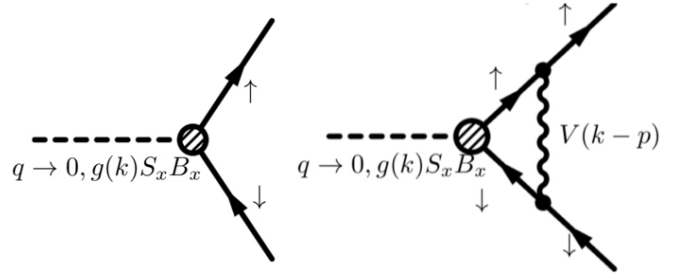


FIG. 1. Left: Feynman diagram for the bare transition moment with an in-plane magnetic field B_x . Right: Vertex diagram associated with the one-loop Coulomb interaction correction shown by the wiggly line $V(\mathbf{p}) = 2\pi e^2/p$.

In the presence of an in-plane magnetic field B_x , the bare transition moment is given by $\mu = \langle \downarrow | S_x | \uparrow \rangle$. Using the above wavefunctions, we calculate the bare transition moment for this model:

$$\mu = \langle \downarrow | S_x | \uparrow \rangle = \frac{k}{\sqrt{k^2 + \lambda^2}}. \quad (5)$$

Basic Feynman diagrams for the bare and one-loop (vertex) correction are given in Fig. 1. Invoking Feynman rules we will write analytic expression corresponding to the vertex function given in the right panel of Fig. 1.

Therefore the one-loop Coulomb interaction correction to the magnetic moment (for $q \rightarrow 0$) is given as

$$\begin{aligned} \delta\mu &= \sum_p i \int \frac{d\omega}{2\pi} \langle \downarrow | G^{s=-1}(p, \omega) S_x G^{s=+1}(p+q, \omega) | \uparrow \rangle \\ &\quad \times V(|\mathbf{p} - \mathbf{k}|) \end{aligned} \quad (6)$$

where, $V(\mathbf{p}) = (2\pi e^2/p)$ is the Coulomb interaction and the corresponding Green's functions for this model is

$$G(\mathbf{k}, \omega) = \frac{\omega + (\sigma \cdot \mathbf{k} + \lambda\sigma_z s_z)}{\omega^2 - \varepsilon_k^2 + i\eta}. \quad (7)$$

Using the above equations along with the the corresponding wave functions (Eq. (3) and Eq. (4)), we derive an expression for the one-loop interaction correction,

$$\delta\mu = \frac{k}{\sqrt{k^2 + \lambda^2}} \alpha \mathcal{W}(k/\lambda), \quad (8)$$

where we have defined,

$$\alpha \mathcal{W}(k/\lambda) = \frac{\lambda^2}{2} \int \frac{d^2 p}{(2\pi)^2} \frac{V(|\mathbf{p} - \mathbf{k}|)}{\varepsilon_p^3} \left(1 - \frac{\mathbf{p} \cdot \mathbf{k}}{k^2} \right), \quad (9)$$

with $\alpha = e^2/\epsilon\hbar v$ as the effective fine-structure constant representing the strength of Coulomb interactions and ϵ is the dielectric constant.

The variation of the correction function $\mathcal{W}(k/\lambda)$ with the dimensionless band momenta (k/λ) is shown in the

top panel of Fig. 2. The Coulomb interaction correction peaks at $k = 0$ and there after decays with the increase in band momenta.

Using Eqs. (5), (8) and (9), we write the total transition moment as,

$$\mu + \delta\mu = \frac{k}{\sqrt{k^2 + \lambda^2}} \left[1 + \frac{\lambda^2}{2} \int \frac{d^2p}{(2\pi)^2} \frac{V(|\mathbf{p} - \mathbf{k}|)}{\varepsilon_p^3} \left(1 - \frac{\mathbf{p} \cdot \mathbf{k}}{k^2} \right) \right]. \quad (10)$$

To display the effects of the Coulomb interaction correction, we show the dependence of the total transition moment $\mu + \delta\mu$ with the dimensionless band momenta for various values of the coupling α . The maximum value of $\alpha = 2.2$ can be achieved in suspended samples while the presence of a substrate leads to screening and thus a decrease of α . We observe that the correction effect increases with the increase in α thereby revealing a strong signature of the effect of Coulomb interaction correction on the transition moment for this model.

In our next section we extend this formalism to calculate the one-loop Coulomb interaction correction for the transition moment in the atomically thin dichalcogenides.

III. ANOMALOUS TRANSITION MOMENT IN ATOMICALLY THIN FAMILY OF DICHALCOGENIDES

In contrast to the Kane Mele model, the atomically thin transition metal dichalcogenides (TMDCs) display a large spin-independent gap (\sim of the order of few eVs) which originates from the broken inversion symmetry of the sublattice of these systems^{14,24}. Along with a large spin independent gap which we refer as Δ , these materials also display strong intrinsic spin-orbit coupling arising from the admixture of the d-orbitals of the transition metals^{24,25}. In this section, we will probe the Coulomb interaction effect on the SOC-induced magnetic moment of these class of materials. Our procedure will be the same as before.

The effective low energy Hamiltonian associated with the monolayer TMDCs¹⁴,

$$H = \sigma \cdot \mathbf{k} + (\Delta/2)\sigma_z - (\lambda/2)(\sigma_z - 1)s_z. \quad (11)$$

Here, Δ is the spin-independent gap and λ is the spin-orbit coupling. The model parameters for MoS₂ are $\Delta \approx 1.66$ eV, $2\lambda \approx 0.15$ eV; for WS₂ are $\Delta \approx 1.79$ eV, $2\lambda \approx 0.43$ eV, and for WSe₂ are $\Delta \approx 1.6$ eV, $2\lambda \approx 0.46$ eV^{14,24} which clearly indicate that the family of TMDCs can be classified by a regime in which the spin-independent gap is much larger compared to the spin-orbit coupling,

$$\Delta/\lambda \gg 1. \quad (12)$$

The exact wave functions at momentum k for these

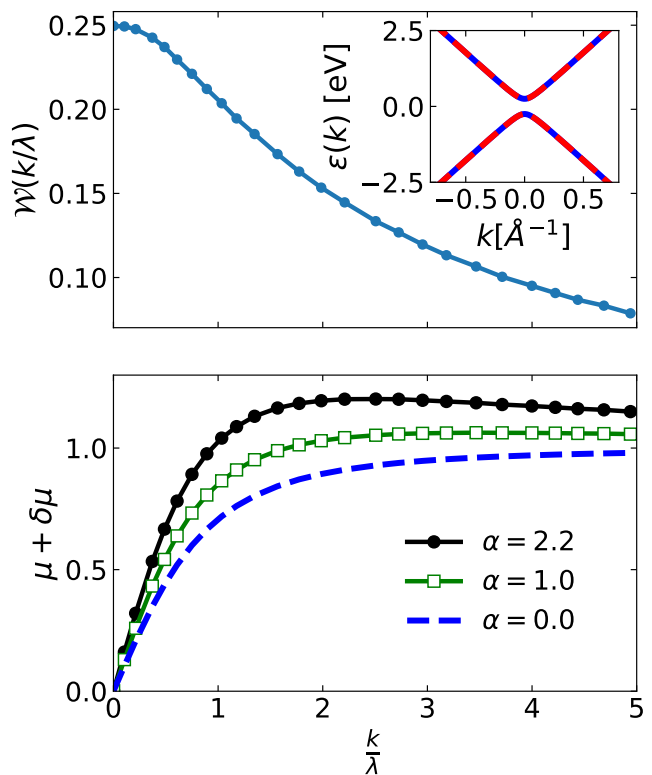


FIG. 2. Top panel: Variation of the correction function $\mathcal{W}(k/\lambda)$ with rescaled momentum k/λ . The magnitude of the correction is large and maximum at $k = 0$. Right inset: Low-energy band structure for the Kane Mele model. Bands spin degenerate with a gap that is generated by the spin-orbit interaction λ . Bottom panel: Variation of the total spin-flip transition moment, $\mu + \delta\mu = \frac{k}{\sqrt{k^2 + \lambda^2}} (1 + \alpha\mathcal{W}(k/\lambda))$, with rescaled momentum (k/λ). With the increase in α we see an enhancement in the total transition moment. We relate this increase to the enlarged correction effects from Coulomb interactions.

class of materials are written as

$$\Psi(k)_n^s = \frac{k}{\sqrt{k^2 + (E_{k,n}^s)^2}} \begin{pmatrix} 1 \\ E_{k,n}^s/(k_x - ik_y) \end{pmatrix}, \quad n = 1, 2 \quad (13)$$

with s as the spin index, $n = 1$ and $n = 2$ labels the conduction band and valence band respectively. Here we have defined $E_{k,n}^s$ as the quantities

$$E_{k,n}^s = \varepsilon_{k,n}^s - \Delta/2, \quad s = s_z = \pm 1. \quad (14)$$

$\varepsilon_{k,n}^s$ represent the eigenenergies:

$$\varepsilon_{k,1}^s = \lambda s/2 + \varepsilon_k^s > 0, \quad n = 1, \quad (15)$$

$$\varepsilon_{k,2}^s = \lambda s/2 - \varepsilon_k^s < 0, \quad n = 2, \quad (16)$$

with ε_k^s appropriately defined:

$$\varepsilon_k^s \equiv +\sqrt{k^2 + [(\Delta - \lambda s)^2/4]}. \quad (17)$$

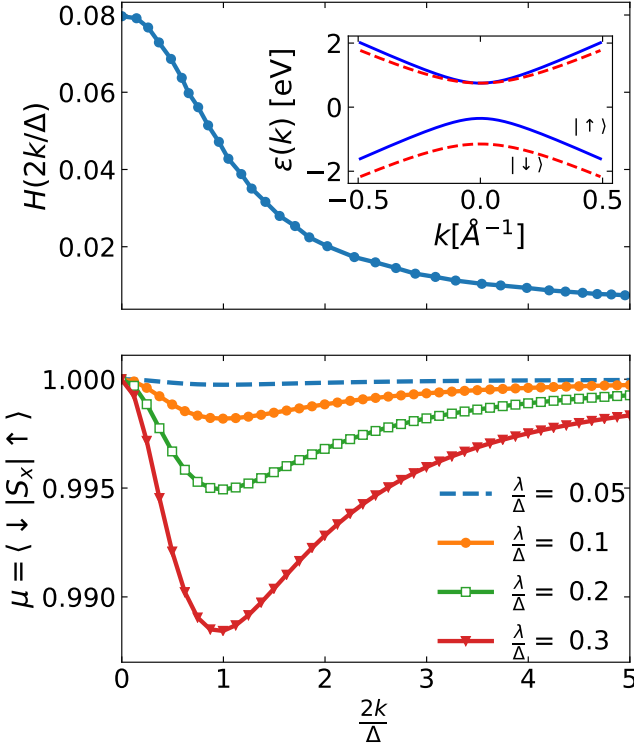


FIG. 3. Top panel: Correction function $H(2k/\lambda)$ for the dichalcogenides. Here, we have used the rescaled momentum: $2k/\Delta$. As can be seen from the figure, at $2k/\Delta = 0$, the value of the correction function $H(2k/\Delta)$ is very small (~ 0.08 .) Inset plot on top panel shows the corresponding dispersion relation for the dichalcogenides. The conduction bands are degenerate at $k=0$ and are also seen to undergo a band inversion. Bottom panel: Bare transition moment for the dichalcogenides for various values of λ/Δ . For TMDCs with the relevant value of $\lambda/\Delta \lesssim 0.15$, we see that the value of μ is almost a constant ≈ 1 and shows negligible variation with the momentum.

In the right inset of top panel of Fig. 3, we show the low-energy band structure for this group of materials corresponding to Eq. (17). These bands are non-degenerate, showing spin inversion with a large spin-independent gap.

The bare transition moment is calculated using the wave functions for the conduction band (given in Eq. (13)) leading to

$$\mu = \langle \downarrow | S_x | \uparrow \rangle = \frac{k^2 + E_{k,1}^+ E_{k,1}^-}{\sqrt{(k^2 + [E_{k,1}^+]^2)(k^2 + [E_{k,1}^-]^2)}}. \quad (18)$$

For the correction to the bare transition moment we will use the vertex function and Eq. (6). The Green's function for this model is

$$G^s(p, \omega) = \frac{1}{2\varepsilon_p^s} \left[\frac{\varepsilon_p^s + \sigma \cdot \mathbf{p} + \sigma_z(\Delta - \lambda s)/2}{\omega - \varepsilon_{p,1}^s + i\eta} - \frac{-\varepsilon_p^s + \sigma \cdot \mathbf{p} + \sigma_z(\Delta - \lambda s)/2}{\omega - \varepsilon_{p,2}^s - i\eta} \right]. \quad (19)$$

Using the above Green's function we first perform the frequency integral in Eq. (6) with the result

$$i \int \frac{d\omega}{2\pi} [G^- G^+] \approx \frac{1}{4\varepsilon_p^+ \varepsilon_p^-} \frac{1}{[\lambda^2 - (\varepsilon_p^- + \varepsilon_p^+)^2]} \left[\lambda^2 \frac{\Delta}{\varepsilon_p} (\sigma \cdot \mathbf{p}) - 2\lambda^2 \frac{p^2}{\varepsilon_p} (\sigma_z + 1) - 4\lambda \varepsilon_p (\sigma \cdot \mathbf{p}) \sigma_z \right]. \quad (20)$$

Here we have expanded the numerator up to $O[\lambda^2]$. The pre-factors of Eq. (20) given by the energy denominators can be taken at $\lambda = 0$ because their expansion starts from a constant and the next order is $O[\lambda^2]$. Following Eq. (6), the interaction correction to the transition moment is derived by taking the expectation value of the above equation with respect to the wave functions $\Psi(k)_1^\pm$ (Eq. (13)),

$$\delta\mu = \sum_{\mathbf{p}} V(k-p) \frac{(-1)}{16\varepsilon_p^4} \lambda^2 \frac{2}{k^2 + E_k^2} \Gamma(p, k), \quad (21)$$

where the function $\Gamma(p, k)$ has been calculated as

$$\Gamma(p, k) = \frac{1}{\varepsilon_p} \left\{ \Delta E_k(\mathbf{k} \cdot \mathbf{p}) - 2p^2 k^2 \right\} + 2\varepsilon_p(\mathbf{k} \cdot \mathbf{p}) \left(1 - \frac{\Delta}{2\varepsilon_k} \right). \quad (22)$$

In the above expression, we have used the following definitions

$$E_k = \varepsilon_k - \Delta/2, \quad \varepsilon_k \equiv \sqrt{k^2 + [\Delta^2/4]}. \quad (23)$$

Finally we derive the total transition moment as the sum of the bare (Eq. (18)) and the Coulomb interaction dependent spin-flip transition moment (Eq. (21)),

$$\mu + \delta\mu = \langle \downarrow | S_x | \uparrow \rangle (1 + \alpha(2\lambda/\Delta)^2 H(2k/\Delta)), \quad (24)$$

where the correction term is conveniently written as

$$\delta\mu = \langle \downarrow | S_x | \uparrow \rangle \alpha(2\lambda/\Delta)^2 H(2k/\Delta), \quad (25)$$

with the function $H(2k/\Delta)$ which can be easily evaluated using Eq. (21) & Eq. (22).

In the top panel of Fig. 3 we show the variation of the Coulomb interaction correction function $H(2k/\Delta)$ with respect to the dimensionless band momenta. We observe that the magnitude of this correction is very small for this class of materials. This can be understood from the fact that the spin-independent gap for these materials overwhelms the contribution from the spin-orbit coupling term.

In the next section, we will derive the anomalous transition moment for the Silicene-Germanene class of materials.

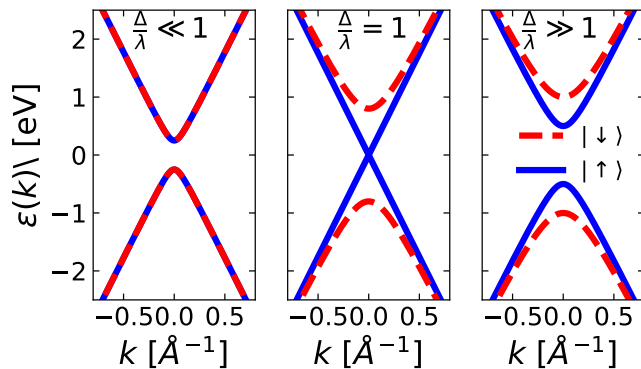


FIG. 4. Dispersion curves for Silicene-Germanene type of materials. With the proper tuning of the ratio of spin-independent gap to spin-orbit coupling (Δ/λ), the band structure shows a transition from a topological insulator ($\Delta \ll \lambda$) to a band insulator ($\Delta \gg \lambda$) via the quantum critical VSPM state ($\Delta = \lambda$). Subsequent removal of the spin degeneracy is also observed for the bulk insulator regime ($\Delta \gg \lambda$).

IV. EFFECT OF COULOMB INTERACTIONS ON TRANSITION MAGNETIC MOMENTS IN SILICENE-GERMANENE CLASS OF MATERIALS

An application of transverse electric field along the staggered sublattices of this class of materials causes the low-energy band structure to evolve from a topological insulator (TI) to a bulk insulator (BI) via a Valley Spin Polarized Metal (VSPM) state^{27,34-37}. In this section, we will first summarize the low-energy band structure of these class of materials and show that the evolution of the low-energy band structure from TI to BI via a VSPM state can also be attained with proper tuning of the dimensionless parameter which represents the ratio of spin-independent gap to the spin-orbit coupling (Δ/λ). This class of materials thus open up the possibility to explore the Coulomb interaction correction for a large parameter regime.

The Hamiltonian of this class of materials^{27,35,36} is

$$H = v\sigma \cdot \mathbf{k} + \frac{(\Delta - \lambda s_z)}{2} \sigma_z. \quad (26)$$

The exact wave functions at momentum k for the Hamiltonian given by Eq. (26),

$$\Psi(k)_n^s = \frac{k}{\sqrt{k^2 + (E_{k,n}^s)^2}} \begin{pmatrix} 1 \\ E_{k,n}^s / (k_x - ik_y) \end{pmatrix}, \quad n = 1, 2 \quad (27)$$

where $n = 1$ labels the conduction band; $n = 2$ labels the valence band. We have defined $E_{k,n}^s$ as:

$$E_{k,n}^s = \varepsilon_{k,n}^s - \frac{(\Delta - \lambda s)}{2}, \quad s = s_z = \pm 1, \quad (28)$$

where the eigenenergies associated with the conduction and valence band are given by $\varepsilon_{k,n}^s$:

$$\varepsilon_{k,1}^s = \varepsilon_k^s > 0, \quad n = 1, \quad (29)$$

$$\varepsilon_{k,2}^s = -\varepsilon_k^s < 0, \quad n = 2, \quad (30)$$

and we use the definition:

$$\varepsilon_k^s \equiv +\sqrt{k^2 + [(\Delta - \lambda s)^2/4]}. \quad (31)$$

Fig. 4 shows the low-energy band structure corresponding to Eq. (31) plotted for three different values of (Δ/λ) $\ll 1$, (Δ/λ) = 1 and (Δ/λ) $\gg 1$. As can be seen the three different cases corresponding to different values of (Δ/λ) are consistent with the TI, VSPM and a BI state. Next, we derive the expression for the bare transition moment using the conduction band wave functions given by Eq. 27.

From Eq. (27), we can write the the corresponding conduction band ($n = 1$) wave functions $|\uparrow\rangle$ and $|\downarrow\rangle$ as:

$$|\uparrow\rangle = \Psi(k)_1^{+1} = \frac{k}{\sqrt{k^2 + (E_{k,1}^+)^2}} \begin{pmatrix} 1 \\ E_{k,1}^+ / (k_x - ik_y) \end{pmatrix} \quad (32)$$

$$|\downarrow\rangle = \Psi(k)_1^{-1} = \frac{k}{\sqrt{k^2 + (E_{k,1}^-)^2}} \begin{pmatrix} 1 \\ E_{k,1}^- / (k_x - ik_y) \end{pmatrix} \quad (33)$$

Using Eq. (32) and Eq. (33), we derive an expression for the band-momentum dependent bare transition moment,

$$\mu = \langle \downarrow | S_x | \uparrow \rangle = \frac{k^2 + E_{k,1}^+ E_{k,1}^-}{\sqrt{(k^2 + [E_{k,1}^+]^2)(k^2 + [E_{k,1}^-]^2)}}. \quad (34)$$

In the top panel of Fig. 5, we show the variation of the bare transition moment $\mu \equiv \langle \downarrow | S_x | \uparrow \rangle$ with a dimensionless rescaled momentum ($2k/\lambda$) for various values of (Δ/λ). The overall variation of the spin flip transition with momentum for different values of the spin-independent gap can be intuitively understood in the following way. At $\Delta/\lambda = 0$, which corresponds to the Kane Mele model, the system is stiff in the spin z direction as the term proportional to s_z favors ordering and thus a transverse field at zero momentum (uniform field) can not cause spin flip, while at finite momentum this becomes possible. In the opposite extreme, $\Delta/\lambda \gg 1$, a spin flip can be achieved effortlessly as the s_z term can be neglected.

Finally we turn to the interaction corrections. The expression for the Green's function $G(\mathbf{k}, \omega)$ corresponding to the Hamiltonian of Eq. (26), reads

$$G(\mathbf{k}, \omega) = \frac{1}{2\varepsilon_k^s} \left[\frac{\varepsilon_k^s + \sigma \cdot \mathbf{k} + \left(\frac{\Delta - \lambda s_z}{2}\right) \sigma_z}{(\omega - \varepsilon_k^s + i\eta)} + \frac{\varepsilon_k^s - \sigma \cdot \mathbf{k} - \left(\frac{\Delta - \lambda s_z}{2}\right) \sigma_z}{(\omega + \varepsilon_k^s - i\eta)} \right]. \quad (35)$$

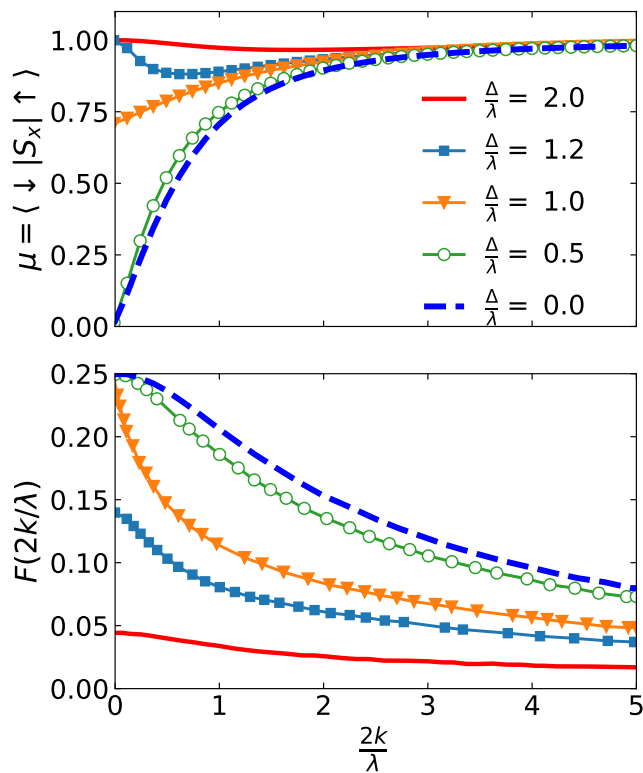


FIG. 5. Top panel: Variation of the bare transition moment $\mu = \langle \uparrow | S_x | \downarrow \rangle$ with the rescaled momentum $2k/\lambda$ for several values of Δ/λ . As the coupling parameter Δ/λ increases the system makes a transition from TI to BI via the VSPM state ($\Delta/\lambda = 1$). Bottom panel: Variation of the correction function $F(2k/\lambda)$ with $2k/\lambda$ for various values of coupling $0 < \Delta/\lambda < 2$. The correction term is seen to be large for the topological insulators ($\Delta/\lambda \ll 1$) compared to the VSPM ($\Delta/\lambda = 1$) or bulk insulators states ($\Delta/\lambda \gg 1$).

We evaluate the frequency integral in Eq. (6) by using the Green's function expression from Eq. (35) resulting in

$$i \int \frac{d\omega}{2\pi} \left[G^- G^+ \right] = \frac{1}{2\varepsilon_p^+ \varepsilon_p^-} \left\{ \frac{1}{(\varepsilon_p^+ + \varepsilon_p^-)} \right\} \left[\varepsilon_p^- \varepsilon_p^+ - (\sigma \cdot \mathbf{p})^2 + \left(\frac{\lambda^2 - \Delta^2}{4} \right) + \lambda (\sigma \cdot \mathbf{p}) \sigma_z \right]. \quad (36)$$

We substitute the above equation along with the conduction band wave functions given by Eqs. (32) and (33) in Eq. (6) to derive the expression for the correction term:

$$\begin{aligned} \delta\mu &= \langle \downarrow | S_x | \uparrow \rangle \sum_{\mathbf{p}} \frac{V(|\mathbf{p} - \mathbf{k}|)}{2\varepsilon_p^+ \varepsilon_p^- (\varepsilon_p^+ + \varepsilon_p^-)} \left[\varepsilon_p^+ \varepsilon_p^- - p^2 + \left(\frac{\lambda^2 - \Delta^2}{4} \right) + \lambda (\mathbf{p} \cdot \mathbf{k}) \left\{ \frac{\varepsilon_k^- - \varepsilon_k^+ - \lambda}{k^2 + E_{k,1}^+ E_{k,1}^-} \right\} \right] \\ &= \langle \downarrow | S_x | \uparrow \rangle \alpha F(2k/\lambda, \Delta/\lambda). \end{aligned} \quad (37)$$

The function $F(2k/\lambda, \Delta/\lambda)$ quantifies the Coulomb interaction correction effects and we have defined it as:

$$\begin{aligned} \alpha F(2k/\lambda, \Delta/\lambda) &\equiv \sum_{\mathbf{p}} \frac{V(|\mathbf{p} - \mathbf{k}|)}{2\varepsilon_p^+ \varepsilon_p^- (\varepsilon_p^+ + \varepsilon_p^-)} \left[\varepsilon_p^+ \varepsilon_p^- - p^2 + \left(\frac{\lambda^2 - \Delta^2}{4} \right) + \lambda (\mathbf{p} \cdot \mathbf{k}) \right. \\ &\quad \left. \times \left\{ \frac{\varepsilon_k^- - \varepsilon_k^+ - \lambda}{k^2 + E_{k,1}^+ E_{k,1}^-} \right\} \right], \end{aligned} \quad (38)$$

with $\alpha = e^2/\epsilon\hbar v$ as the effective fine-structure constant that gives the strength of the interactions.

Using Eq. (34) and Eq. (37), we write the expression for the total spin-flip transition moment as

$$\mu + \delta\mu = \langle \downarrow | S_x | \uparrow \rangle \left\{ 1 + \alpha F(2k/\lambda, \Delta/\lambda) \right\}. \quad (39)$$

To assess quantitatively the effect of the Coulomb interaction as a function of the band momentum, we plot the variation of the function $F(2k/\lambda)$ with the rescaled momentum ($2k/\lambda$) for several values of (Δ/λ) in the bottom panel of Fig. 5. The correction function is seen to be maximum at $k = 0$ for all the different values of (Δ/λ) and is seen to decrease with increasing values of the band momenta. Although for ($\Delta/\lambda \leq 1$) the bare transition moment μ was found to be 0 at $k = 0$, the Coulomb interaction correction effects turn out to be the largest for this regime. However increasing the value of (Δ/λ) leads to a decrease in the Coulomb interaction correction. Of course the correction function $F(2k/\lambda)$ has to be multiplied by the dimensionless Coulomb interaction strength $\alpha \sim 1$ which is strongly material and environment dependent. It is clear from Fig. 5 that the overall interaction effect is strongest in the parameter regime $\Delta/\lambda \approx 0$, i.e. in the Kane Mele universality class, while for $\Delta/\lambda > 1$ and beyond the correction becomes gradually smaller and less pronounced even for substantial values of α as the system becomes dominated by the spin-independent gap.

V. DISCUSSION AND OUTLOOK

In summary we have analyzed, for the first time, the effect of Coulomb interactions on the spin transition magnetic moment for the case of atomically thin hexagonal lattices with spin-orbit interactions, such as 2D topological insulators (described by the Kane Mele Model), dielectric group-VI Dichalcogenides and the Silicene-Germanene class of materials. Due to the non-relativistic nature of these systems, and because of the two-dimensional nature of all the studied materials (meaning that the spin-orbit interaction is a relatively small effect on top of the band structure), the ‘‘anomalous’’, i.e. Coulomb interaction effect manifests itself anisotropically, and indeed only in the spin-flip channel,

for magnetic fields in the material planes. This is in contrast (although conceptually and technically very similar in spirit) to the famous anomalous magnetic moment of the electron in relativistic QED where the Schwinger result renormalizes directly and isotropically the electron g -factor. We can view our results as yet another important manifestation of (moderately strong) electron-electron interaction effects in graphene-like hexagonal monolayer systems which exhibit Dirac quasiparticle spectra.

We also note that in our calculations we have confined ourselves to the first nontrivial order in the interaction strength (α), which is justified by the relative smallness of the corrections. One can take into account higher order effects in various approximation schemes; for example as a first observation we point out that the coupling α itself is renormalized by interactions (and decreases as the renormalization energy scale decreases)⁴. This is expected to somewhat decrease further the effects discussed in this paper, although by exactly how much depends on the details of the system and the energy (momentum) at which one calculates the magnetic response, as is evident from all the figures in the main part of the paper.

As discussed in the previous section which contains results across all parameter regimes (Fig. 5), it appears that the Kane Mele limit (i.e. no spin-independent gap, but a gap induced by the spin-orbit interaction) represents the point in parameter space where the Coulomb corrections are the strongest (Fig. (2)). On the other hand there has been a significant surge of experimental efforts in studying monolayer dichalcogenides by advanced magneto-optical techniques³⁸. In particular these systems tend to exhibit strong Coulomb effects in the excitonic channel. Unfortunately, even though α could be even larger than graphene's (due to the smaller quasiparticle velocity), these materials have relatively large gaps and reside firmly in the parameter regime $\Delta/\lambda > 1$ which makes the anomalous effects much smaller and therefore harder to detect (see the relevant Fig. 3). Still, it is worth asking the question: what experimental technique

is most suitable to detect anomalous spin contributions? A very promising and highly advanced magneto-optical technique is the one based on the Hanle effect where the spins are manipulated by inducing a spin precession by an in-plane magnetic field³⁸⁻⁴². Spins are excited into the conduction band (which is filled with a finite (small) density of electrons) across the gap and thus prepared in a state with given s_z . Then they are subjected to in-plane magnetic fields and the magnetization relaxation is monitored as a function of the field, exhibiting a characteristic Lorentzian shape. It is then possible, in principle, to estimate and possibly measure the effect of anomalous transition moment on the Hanle curves, as such anomalous contributions would tend, theoretically, to decrease the relaxation times. An accurate description of this effect however is strongly dependent on the particular experimental setup (which involves the exact electron density, screening, precise parametrization of the spin relaxation mechanisms which are at play, etc.) and thus we have not attempted to disentangle our universal anomalous contribution from a given experiment's specific details. We also keep in mind that due to advances both in materials science and experimental techniques, it is quite possible that eventually access to experiments which explore different points in the three-parameter space (spin-orbit interaction, Coulomb interaction, spectral gap) can become feasible.

ACKNOWLEDGMENTS

SS is grateful to Prof. Ion Garate for insightful discussion during the initial formulation of this work. SS was funded by the Canada First Research Excellence Fund. VNK gratefully acknowledges the financial support of the Gordon Godfrey visitors program at the School of Physics, University of New South Wales, Sydney, during two research visits.

¹ A. H. Castro Neto, F. Guinea, N. M. R. Peres, K. S. Novoselov, and A. K. Geim, *Rev. Mod. Phys.* **81**, 109 (2009).

² M. I. Katsnelson, K. S. Novoselov, and A. K. Geim, *Nature Physics* **2**, 620 (2006).

³ M. Katsnelson and K. Novoselov, *Solid State Communications* **143**, 3 (2007).

⁴ V. N. Kotov, B. Uchoa, V. M. Pereira, F. Guinea, and A. H. Castro Neto, *Rev. Mod. Phys.* **84**, 1067 (2012).

⁵ K. Novoselov, A. Geim, S. Morozov, D. Jiang, M. Katsnelson, I. Grigorieva, S. Dubonos, and A. Firsov, *Nature* **438**, 197 (2005).

⁶ Y. Zhang, Y.-W. Tan, H. L. Stormer, and P. Kim, *Nature* **438**, 201 (2005).

⁷ A. Chen, R. Ilan, F. de Juan, D. I. Pikulin, and M. Franz, *Phys. Rev. Lett.* **121**, 036403 (2018).

⁸ V. P. Gusynin and S. G. Sharapov, *Phys. Rev. Lett.* **95**, 146801 (2005).

⁹ Y. Zheng and T. Ando, *Phys. Rev. B* **65**, 245420 (2002).

¹⁰ M. Offidani and A. Ferreira, *Phys. Rev. Lett.* **121**, 126802 (2018).

¹¹ S. Murakami, *Phys. Rev. Lett.* **97**, 236805 (2006).

¹² C. L. Kane and E. J. Mele, *Phys. Rev. Lett.* **95**, 226801 (2005).

¹³ K. S. Novoselov, D. Jiang, F. Schedin, T. J. Booth, V. V. Khotkevich, S. V. Morozov, and A. K. Geim, *Proceedings of the National Academy of Sciences* **102**, 10451 (2005), <https://www.pnas.org/content/102/30/10451.full.pdf>.

¹⁴ D. Xiao, G.-B. Liu, W. Feng, X. Xu, and W. Yao, *Phys. Rev. Lett.* **108**, 196802 (2012).

¹⁵ S. Cahangirov, M. Topsakal, E. Aktürk, H. Şahin, and S. Ciraci, *Phys. Rev. Lett.* **102**, 236804 (2009).

- ¹⁶ P. Vogt, P. De Padova, C. Quaresima, J. Avila, E. Frantzeskakis, M. C. Asensio, A. Resta, B. Ealet, and G. Le Lay, *Phys. Rev. Lett.* **108**, 155501 (2012).
- ¹⁷ M. Z. Hasan and C. L. Kane, *Rev. Mod. Phys.* **82**, 3045 (2010).
- ¹⁸ C. L. Kane and E. J. Mele, *Phys. Rev. Lett.* **95**, 146802 (2005).
- ¹⁹ Y. Yao, F. Ye, X.-L. Qi, S.-C. Zhang, and Z. Fang, *Phys. Rev. B* **75**, 041401 (2007).
- ²⁰ H. Min, J. E. Hill, N. A. Sinitsyn, B. R. Sahu, L. Kleinman, and A. H. MacDonald, *Phys. Rev. B* **74**, 165310 (2006).
- ²¹ V. B. Berestetskii, E. M. Lifshitz, and L. P. Pitaevskii, *Quantum Electrodynamics (Landau and Lifshitz Vol. 4)* (Butterworth-Heinemann, England, 1982).
- ²² J. Schwinger, *Phys. Rev.* **73**, 416 (1948).
- ²³ E. C. I. van der Wurff and H. T. C. Stoof, *Phys. Rev. B* **94**, 155118 (2016).
- ²⁴ H. Hatami, T. Kernreiter, and U. Zülicke, *Phys. Rev. B* **90**, 045412 (2014).
- ²⁵ H. Hatami, T. Kernreiter, and U. Zülicke, *Phys. Rev. B* **90**, 045412 (2014).
- ²⁶ M. Ezawa, *Phys. Rev. B* **86**, 161407 (2012).
- ²⁷ C. J. Tabert, J. P. Carbotte, and E. J. Nicol, *Phys. Rev. B* **91**, 035423 (2015).
- ²⁸ L. Stille, C. J. Tabert, and E. J. Nicol, *Phys. Rev. B* **86**, 195405 (2012).
- ²⁹ C. J. Tabert and E. J. Nicol, *Phys. Rev. Lett.* **110**, 197402 (2013).
- ³⁰ C. J. Tabert and E. J. Nicol, *Phys. Rev. B* **87**, 235426 (2013).
- ³¹ C. J. Tabert and E. J. Nicol, *Phys. Rev. B* **88**, 085434 (2013).
- ³² C. J. Tabert and E. J. Nicol, *Phys. Rev. B* **89**, 195410 (2014).
- ³³ C. J. Tabert, J. P. Carbotte, and E. J. Nicol, *Phys. Rev. B* **91**, 035423 (2015).
- ³⁴ Z. Ni, Q. Liu, K. Tang, J. Zheng, J. Zhou, R. Qin, Z. Gao, D. Yu, and J. Lu, *Nano Letters* **12**, 113 (2012), pMID: 22050667, <http://dx.doi.org/10.1021/nl203065e>.
- ³⁵ M. Ezawa, *Phys. Rev. B* **86**, 161407 (2012).
- ³⁶ M. Ezawa, *The European Physical Journal B* **85**, 363 (2012).
- ³⁷ N. D. Drummond, V. Zólyomi, and V. I. Fal'ko, *Phys. Rev. B* **85**, 075423 (2012).
- ³⁸ L. Yang, N. A. Sinitsyn, W. Chen, J. Yuan, J. Zhang, J. Lou, and S. A. Crooker, *Nature Physics* **11**, 830 (2015).
- ³⁹ M. Furis, D. L. Smith, S. Kos, E. S. Garlid, K. S. M. Reddy, C. J. Palmstrm, P. A. Crowell, and S. A. Crooker, *New Journal of Physics* **9**, 347 (2007).
- ⁴⁰ N. Tombros, S. Tanabe, A. Veligura, C. Jozsa, M. Popinciuc, H. T. Jonkman, and B. J. van Wees, *Phys. Rev. Lett.* **101**, 046601 (2008).
- ⁴¹ N. Tombros, C. Jozsa, M. Popinciuc, H. T. Jonkman, and B. J. van Wees, *Nature* **448**, 571 (2007).
- ⁴² S. P. Dash, S. Sharma, J. C. Le Breton, J. Peiro, H. Jaffrès, J.-M. George, A. Lemaître, and R. Jansen, *Phys. Rev. B* **84**, 054410 (2011).